Innovative Vehicle Battery Pack Design Approach through Multiphysics Cells Simulation

Innovative vehicle battery pack design approach through multiphysics cells simulation

Abstract

This paper presents the design procedure of a vehicle battery pack, in terms of electrical and mechanical requirements with an innovative methodology to model Li-ion cells' thermo-electro-mechanical behavior.
A toroidal battery pack was developed for a widespread A-segment vehicle and designed to be placed in the spare wheel compartment.
A novel FEM modelling approach is studied to predict if short circuits happen in case of vehicle crash, avoiding battery pack structure over-engineering. Thus, the classical approach in which cells were treated as a rigid and non-deformable block is overcome.
At the beginning, the toroidal battery pack was sized considering a mild hybrid vehicle conversion. Then, the internal modules layout was defined including also electric connection and cooling system. Subsequently, a benchmarking activity on existing FEM modelling methodologies of single cells was conducted and two approaches were identified and compared: the layer resolved approach, in which every layer composing the cell is modelled and the homogeneous approach, in which all the layers that made up the cells are modelled as an equivalent component.
Considering the literature approaches, three common experimental tests on a single cell were chosen and replicated in LS-DYNA (using the two previous mentioned models) to evaluate the correlation accuracy and the computational costs. Moreover, the calibration of thermo-electro-mechanical coupling was done by defining the short circuit occurrence with an equivalent Von Mises stress threshold.
Finally, the battery pack was validated according to two international standard mechanical tests through a complete full-scale simulation. Pros and cons of this novel modelling approach and its potential application on full-vehicle simulations are presented and discussed.

Introduction

In December 2020 the European Union updated the targets that had been defined two years earlier in the "Paris Agreements", making them more stringent. In this treaty [1] the UN Framework Convention on Climate Change had focused on global pollution and possible way for limiting CO_2 emissions.
The contribution of transport, in Europe, accounts for about 30% and, moreover, unlike other fields, in the last 25 years this value has increased [2]. About it, the EU has decided to set very strict limits of CO_2 g/km for the new car homologation (target for 2020-2025 95 g/km of CO_2 [3]). This encourages the sale of hybrid and electric cars instead of the thermal ones. At the same time, the circulation of obsolete cars has been hampered in favor of less polluting vehicles.
In this scenario, one possible solution to minimize the environmental impact of the current fleet of cars on the road proposing the solution of electric retrofit, that is the modification of an existing vehicle through the introduction of an electric powertrain.
The electrification of existing vehicles is not new, it is already largely carried out both for vehicles equipped for specific tasks to operate in particular areas (urban centers, indoor environments) [4] either for the recovery or transformation of vintage vehicles [5]. As a result, working on a one-off example, costs could be high, changes can be substantial and especially the battery pack is developed ad hoc.
In this paper, a toroidal battery pack has been designed with a shape suitable for the spare wheel space, present on many vehicles. For this reason, an existing city car was considered as case study and a mild-hybrid conversion proposed.
Usually, the design process of a battery pack consists in the definition of a case integrated within the available space of the car, even though the integration of battery pack in the spaceframe could provide several benefits [6]. This process requires the redefinition of the packaging and the homologation through a series of expensive destructive tests, for each new product.
At the same time, battery pack simulation is really challenging due to the number and the small dimensions of the components necessary to evaluate, for instance, short circuit occurrence during a full-vehicle crash. Current solutions avoid deep cell modelling, so the battery pack is considered safe if the case does not surpass a specific displacement

threshold due to an intrusion. An example is presented in [7, 8], where this threshold is carried out by experimental tests performed on a single cell and then corrected by a safety factor.
Another modelling approach is reported in [9], where the battery pack acts not only as energy storage, but also as additional passive safety structure.
However, also in this case the cells are not modelled, and the battery pack overall behavior is simulated with a linear elastic material law or a foam law depending on the battery pack architecture. Failure of the cells is checked considering the principal stresses of the elements made up by this equivalent material and comparing it with a defined threshold.
In this paper, an innovative multiphysics approach is studied to improve the simulation quality of battery pack FEM models, by simulating the impact tests with deformable cells. More specifically, two different cell's modelling strategies are compared in terms of accuracy and computational cost.
Hence, a suitable model for a full vehicle crash simulation is generated by adopting the best modelling approach.
The selected mechanical FE model is coupled with the thermo-electrical solver by using specific advanced LS-DYNA tools and the generated thermo-electro-mechanical FEM model is used to validate the designed battery pack. Finally, a discussion on the methodology pros and cons evaluation is provided, together with the battery pack results.

Battery pack design

Initial assumptions and battery pack architecture

The development of a battery pack needs the definition of specific technical requirements that determine the size and the volume of the external case. For this reason, a widespread A-segment vehicle was selected as case study and its mission as city car was considered for the definition of the electric powertrain.
A mild-hybrid conversion is proposed, considering the installation of two electric motors placed in the rear wheels, as shown in Figure 1.

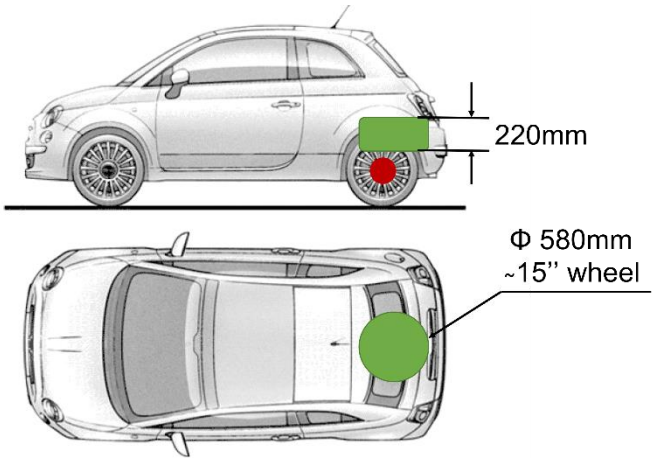

Figure 1. Fiat 500 hybridization scheme, red circle represents motor positioning while green circle represents the battery placement

The parameters showed in the Table 1 are the main requirements.

Table 1. Battery pack main requirements

Technical parameter	Reference value
Rated voltage	600 V
Rated energy	7.25 kWh

Peak power	40 kW
Peak current	66 A

Cylindrical cells were chosen for the toroidal shaped battery pack, since they present the best energy density and structural strength. Its mechanical properties increase the safety of the battery pack both at the level of breaking cells and regarding the loss of electrolyte (required by safety Regulations UNECE R100 [10]).
First, the cell size was selected, and the 21700 format is chosen due to the higher energy density, as shown in Figure 2. Then the electrical sizing was carried out obtaining, with about 500 elements, a mass close to 32 kg.

Figure 2. The cylindrical 21700 battery cell

The battery pack is organized considering the characteristics of the BMS (Battery Management System), for this reason, the cells were placed on 2 floors composed by 7 modules each, as shown in Figure 3.

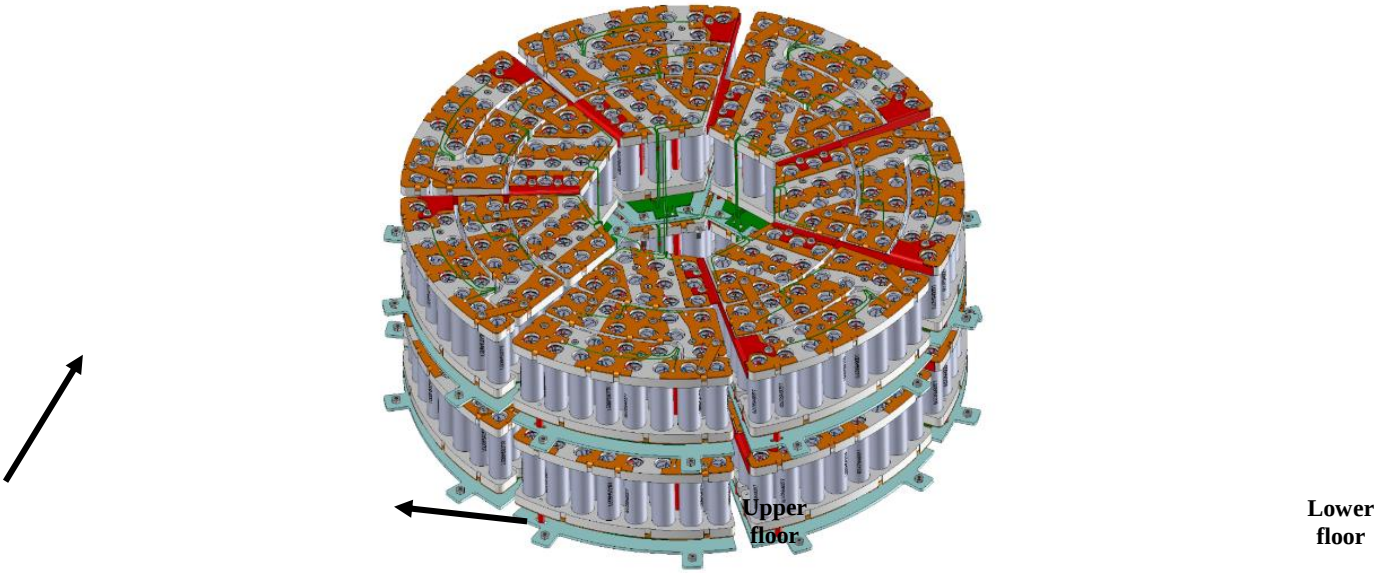

Figure 3. Complete battery pack structure layout including active components

Dividing the battery pack into two identical floors allows the reduction in the design complexity and modularity of the battery pack. Figure 4 depicts a detailed battery pack module.

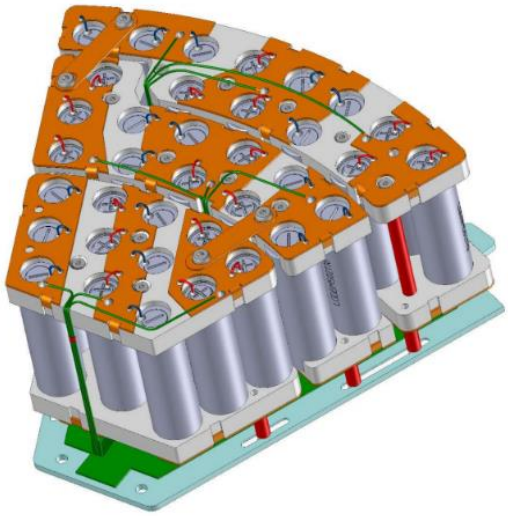

Figure 4. Battery pack module detail with main plastic structure, current collectors and relative BMS board (in green)

The cells' supports were designed in PMMA, as shown in Figure 5, whose mechanical strength, electrical and thermal insulation and flame behavior are compliant with the application.

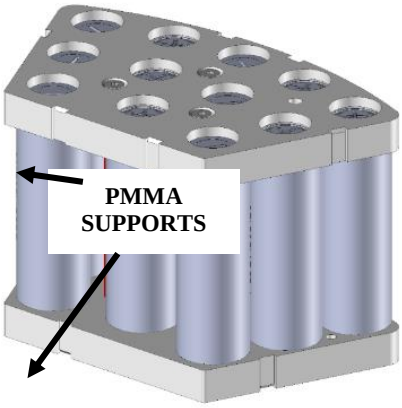

Figure 5. Battery pack sub-module detail, with cells, relative supports and connecting elements

The copper current collectors (Figure 6) and bus bars were designed following the typical electric current values. Moreover, the production process was defined by using laser cutting and bending, as well as the assembly scheme and the bus bar are insulated by a resin coating where needed.

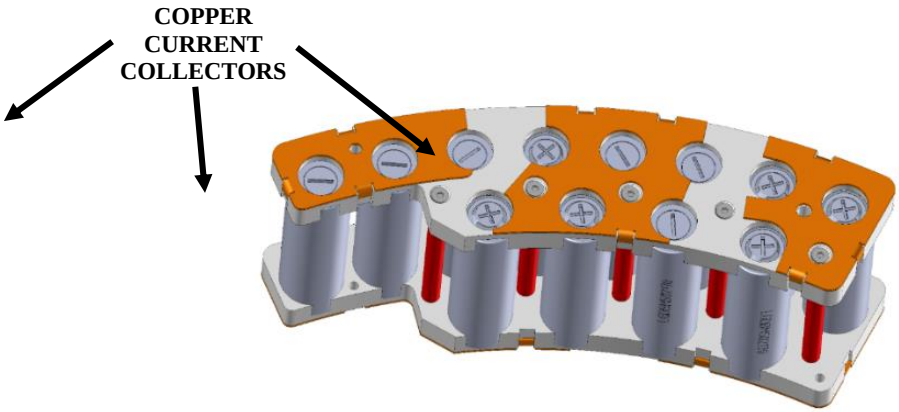

Figure 6. Current collectors' detail with power connections elements

In case of the impossibility to make power connections via bus bar connectors, cables of appropriate section were adopted. These elements allow the simple disconnection of the different sections of the package, facilitating the assembly and disassembly operations.
As concerns the outer case, it was conceived as the union of two separate elements, in which every single cell floor has been stored.
These two components have been connected through bolt and seals at their interface (Figure 7).

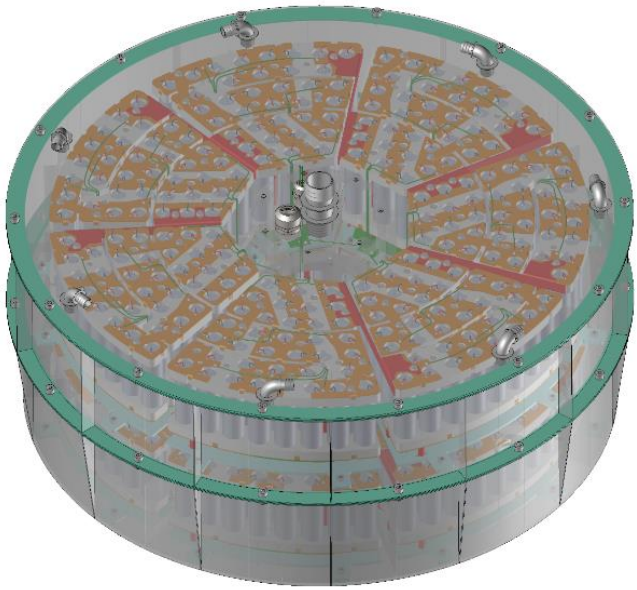

Figure 7. Toroidal battery pack with relative seal (in green)

The best trade-off between structural requirements, construction simplicity, lightness and cost was investigated. Indeed, the entire structure consists of steel sheets of different thicknesses, rolled and welded to obtain the metallic case as light and resistant as possible.
The complete modules are housed in special sections arranged inside each floor. In this way, the septa contribute also to the structure's stiffness and strength, and external radial solicitations result in a load path that passes through the septa themselves, pass around the internal cylinder and discharge again along the septa, as can be seen in Figure 8.

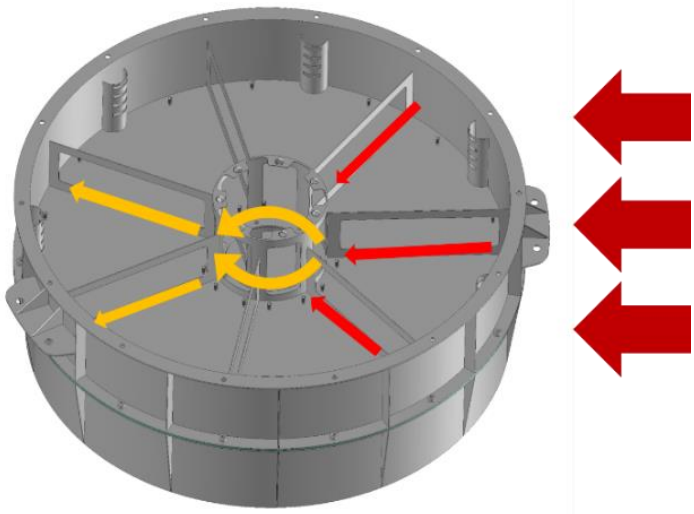

Figure 8. Force lines distribution during a radial impact

In addition, the external flanges placed in the outer cylinder enhance the circumferential integrity of the battery pack both in static and in crash conditions.
It can also be noted that the two semi-houses, lower and upper, are bolted through two series of screws, as showed in Figure 9.

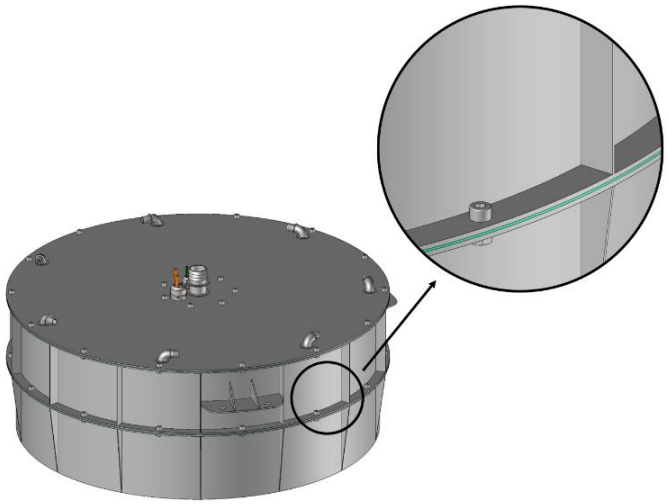

Figure 9. Battery pack upper and lower semi-houses and connecting flanges with relative screws

Cooling system

A preliminary cooling system design was also considered to guarantee a controlled operational environment for each cell module. Because no thermal calculations were done in this stage, some assumptions have been carried out in relation to existing electrothermal model [11, 12]. A dielectric coolant was chosen as carrier and convective motion principle have been considered to remove heat. The system is equipped with 7 inlets arranged on the lid connected with the cell modules. The coolant, guided by the partitions through the module is pushed to the central column tube removing heat. The working scheme is shown in Figure 10.

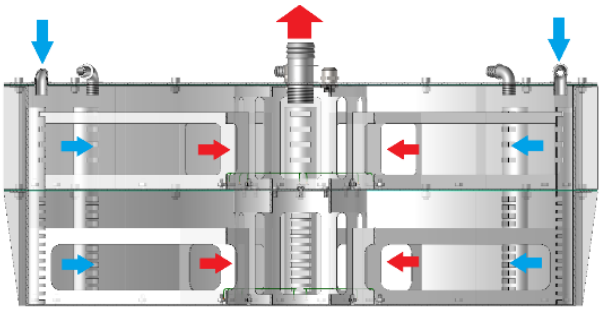

Figure 10. Cooling system working scheme: blue arrows entering refrigerant cold fluid and red arrows exiting refrigerant heated fluid

Battery pack structural simulations

Cell FEM models evaluation and definition

The structural verification of the battery pack was the second main step of the design phase. First, the definition of the single FE cell model was studied. LS-Dyna (R12) solver was used for all the simulation conducted, while ANSA BetaCAE was used to set up all the FEM models.
The creation of a detailed FE cell model is very challenging due to the small component's dimensions and thicknesses, as reported in Table 2.

Table 2. Main battery components thicknesses

Component	Material	Typical thickness (µm)
Cover sheet	Polyamide	120
Copper layer	Copper foil	11
Anode	Graphite	65
Separator	Polypropylene	25
Cathode	LiMn0.3Ni0.3Co0.3O2	80
Aluminium layer	Aluminium foil	19

The existing FEM modelling approach found in literature can be divided mainly into two groups: the layer resolved method and the homogeneous one.
Two layer resolved models of pouch cells are shown in [13] and [14]. Through this method, each layer or each component of the cell is modelled: sometimes the current collectors and the active parts (graphite and lithium metal oxide) are considered as made up by a unique equivalent material due to the difficulties of getting reliable experimental results. Active materials properties were carried out from [15], defined as a difference of the tensile mechanical behavior between the current collectors with and without the active materials spread on them. In contrast to the layered resolved method, the homogenous approach used in [16, 17 and 18] consists in the characterization of the whole cell or the jellyroll as if they were made of an equivalent material. Due to the porosity of active materials and the separator, the material laws typically implemented are that one used for the foams. To verify the two models' capabilities in terms of accuracy and computational cost, the simulation of three experimental tests have been performed on a single cylindrical cell.
For this reason, in this paper the experimental tests performed in [18] have been considered as reference and they have been replicated virtually as showed in Table 3.

Table 3. Experimental tests description

Test	Description
Cylindrical rod indentation	Compression between flat plate and indenter with 8 mm radius
3-points bending	10 mm diameter indenter pushes in the middle of the cell that is supported by two semicircular support of 24 mm diameter

Hemispherical indentation	Cell is pressed between a hemispherical indenter with 12.7 mm diameter and a flat plate

The first model presented is the layer resolved implementation of the cylindrical cell, shown in Figure 11. Shell elements were used for the cell case modelling (red component in the FEM model), while solid brick elements were used for the jellyroll. The cell extremities were kept open to avoid bad quality elements and very small timestep. The internal structure was simplified to reduce meaningless complexities. In fact, the jellyroll has been modeled with concentric cylinders made up by the different materials instead of its spiral shape (right side of Figure 11), although some stiffening effects could occur during the simulation.

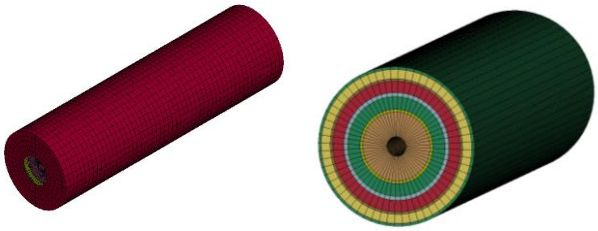

Figure 11. Layer resolved FEM model of the cylindrical cell (left) and jellyroll of the same model (right)

The material calibration of the layer resolved model was conducted on a pouch cell made of similar chemistry reported in [17], and the model used to replicate that cell is depicted in Figure 12.

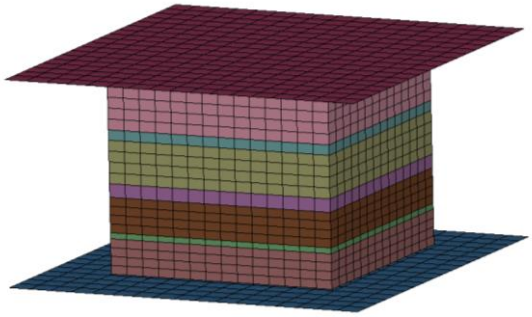

Figure 12. Layer resolved specimen FEM model for material data calibration

The fitting procedure is performed considering known the aluminum and the copper laws, modelled in LS-DYNA through the MAT_SIMPLIFIED_JOHNSON_COOK material card (MAT_098). The selected parameters are listed in Table 4. Starting from the left columns are shown: the density ρ, the Young modulus E, the Poisson ratio v, the yielding stress A, strain hardening related parameters B and n and finally the strain-rate dependent parameter C.

Table 4. Copper and Aluminium input cards main parameters

Material	**ρ [kg/m³]**	**E [GPa]**	**N**	**A [GPa]**	**B [GPa]**	**n**	**C**
Copper	8960	117	0.33	0.09	292	0.31	0.025
Aluminium	2700	69	0.29	0.265	426	0.34	0.015

Instead, the material laws for the active materials and the separator was tuned by using the MAT_CRUSHABLE_FOAM card (MAT_063).

The MAT_063 material card requires input curves for what concerns the compression: this allows more flexibility in the stress-strain relationship definition. For this reason, a power law curve is generated with parameter showed in equation 1.

$$\sigma = 400\varepsilon^{1.75} \tag{1}$$

As results, the obtained material cards were included into the layer resolved model of the cylindrical cell.
In Figure 13 is shown the homogeneous model of the cylindrical cell, where the jellyroll (in blue) is considered as a singular component.

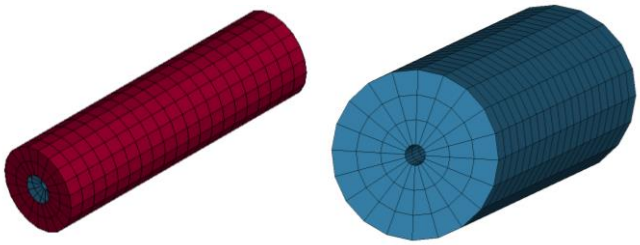

Figure 13. Homogeneous FEM model of the cylindrical cell (left) and jellyroll of the same model (right)

Material data presents in [18] have been considered as input for the jellyroll homogeneous model. Also in this case, the law adopted to simulate the equivalent homogenous material is the MAT_63 CRUSHABLE_FOAM, whose compression behavior has been tuned by the equation 2 and to better fit experimental results.

$$\sigma = 550\varepsilon^{2} \tag{2}$$

When materials are modelled with CRUSHABLE_FOAM they are supposed to be isotropic. Obviously, cells' jellyroll is not isotropic, but this assumption has been validated by the final correlation results.

Main approaches comparison

As explained before, three experimental tests have been selected from [18] and illustrated in Figure 14. All the simulations were run using the same parameters in the same calculation server, which has four Intel Xeon Gold 6254 3.1 GHz processors.
The objective of these comparisons is to find a single cell model that is able to fit simultaneously the three experimental tests with the highest accuracy level, together with the lowest computational cost.

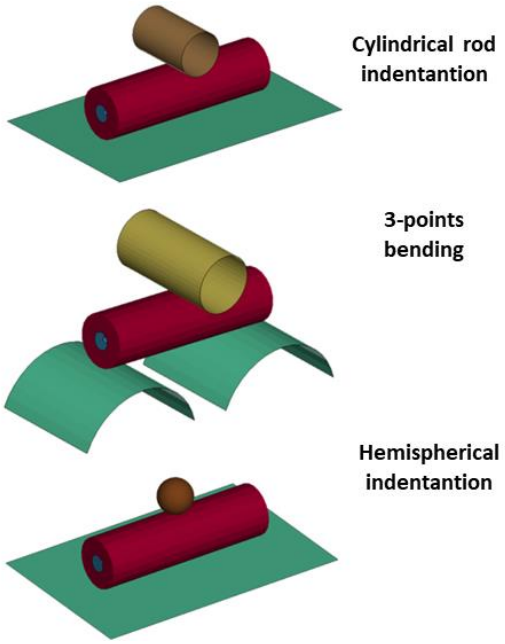

Figure 14. Three FEM model of the experimental tests: lateral indentation, 3-point bending and hemispherical indentation

Figure 15 shows the results in terms of force versus displacement for the cylindrical rod indentation, 3-points bending and the hemispherical indentation respectively.
A good level of correlation is obtained for what concerns the homogeneous model in the cylindrical rod indentation and the hemispherical indentation.
On the contrary, the 3-point bending simulation results stiffer than the experiments, probably due to the larger element size and the difficulty to correctly reproduce the flexural behavior with the material law.
However, the cylindrical rod indentation and the hemispherical indentation are considered more relevant, due to cell assembly scheme, that reduce the chance of flexural behavior in case of impact.
A different situation appears for the layer resolved model, because the three simulations were not able to follow the force-displacement characteristics from a certain displacement. In fact, the FEM curves of the two indentations follow very well the experimental trends until 3,5 mm, while after they become no more reliable with a consistent stiffness variation. This problem may be linked to two factors: the first one linked to the material models adopted and their difficulties to be properly calibrated for each layer. The second one, is related to the SOC (State of Charge): as discussed in [19], fully charged cells can be up to 30% stiffer than fully discharged ones. Nevertheless, the three-point bending virtual curve has a better behavior than the homogeneous one.

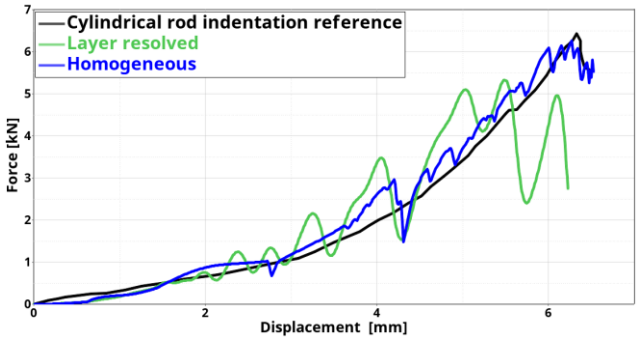

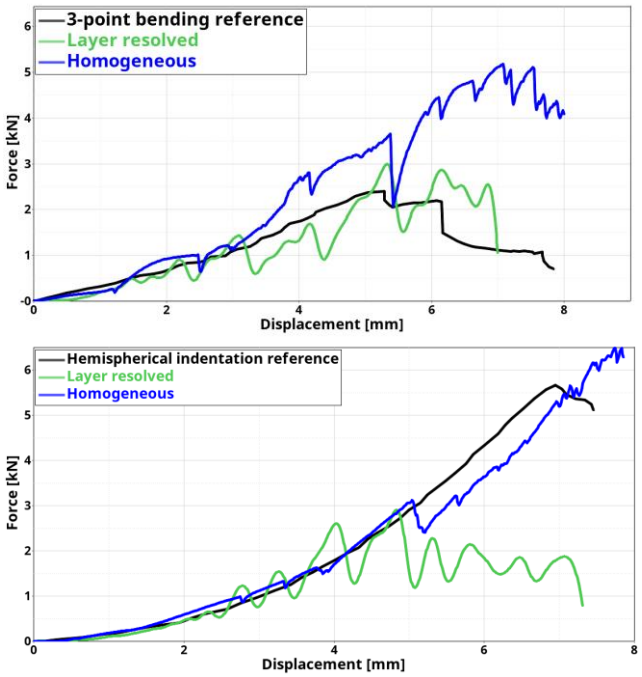

Figure 15. Force vs. displacement comparison between the two FEM model, the experimental test and the FEM literature model for lateral indentation, 3-point bending and hemispherical indentation cases

In addition to the correlation results, in Table 5 are reported computational costs of the two different approaches comparing elements typologies and numbers, timesteps and simulation times. The results show that the layer resolved model for a single cell simulation is dramatically time demanding with respect to the homogenous one, and, as consequence, a full battery pack simulation would require a large computational effort at full vehicle scale.

Table 5. Main FEM model and simulation parameters

	Homogeneous	**Layer resolved**
Shell elements for case	480 elements	2600 elements
Hexa elements for jellyroll	1200 elements	58080 elements
Initial time step	2.24 E-04 ms	9.57 E-05 ms
Simulation time lateral indentation	18m 6s	17h 21m 39s
Simulation time three-point bending	18m 51s	18h 02m 11s
Simulation hemispherical indentation	18m 23s	17h 32m 54s

Since the accuracy reached by the homogeneous model is higher than the layer resolved it was considered more suitable for the complete battery pack simulations. Furthermore, the homogeneous model has a suitable timestep and computational cost in comparison to a full vehicle simulation.
The layer resolved model timestep is considerably smaller than the homogeneous one because the maximum element size is constrained by the thicknesses of the concentric cylinders, otherwise the overall cell mass would be different from the real cell. Instead, for the homogeneous model, the element thickness constraints are only related to the physical cell dimensions and the mesh quality indexes.
In conclusion, for the scope of this paper the homogenous approach represents the best trade-off between computational costs, accuracy and model detail levels.

Cell Multiphysics model: the thermo-electro-mechanical coupling

After the cell mechanical model definition, the thermal and electromagnetic models have been studied. The KEYWORD used for the implementation of the electromagnetic modelling is the RANDLE_BATMAC one, which places an equivalent circuit (Figure 16) in each node of the jellyroll mesh. The equivalent circuit can have different number of parallel resistors and capacitors depending on the order of the circuit.

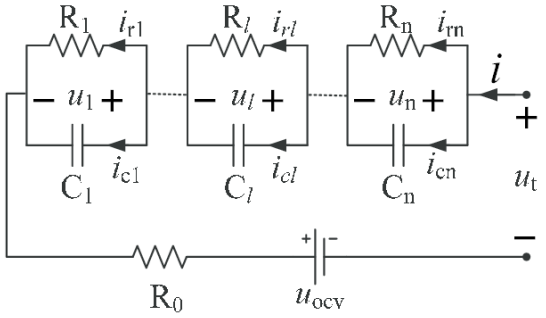

Figure 16. Third order Randle equivalent circuit scheme

Equivalent circuit parameters are obtained through charging-discharging experimental tests, these parameters are a function of different cell properties that changes in time (like temperature, SOC and current direction). In this paper they are considered constant with values as in Table 6.

Table 6. Second order Randle circuit parameters

R_0 [ohm]	R_1 [ohm]	R_2 [ohm]	C_1 [Farad]	C_2 [Farad]
0.07	0.03	0.01	800	1730

The electro-mechanical coupling is obtained through the KEYWORD RANDLE_SHORT, which causes a short circuit to occur. This function can be defined in relation to a stress or a strain threshold, that if exceeded causes a short circuit occurrence modelled by substituting the equivalent circuit with a small resistance. The strain threshold could be a good choice since it has “permanent effect” which is an advantage in case of large deformations. However, the current software version does not allow to postprocess the related strain outcomes.
Therefore, a specific methodology has been adopted to assess the threshold stress value in relation to the accuracy between experimental outcomes and simulation results at the short circuit occurrence. In Figure 17, the comparison

between the experimental and FEM energy absorbed are plotted in relation to the indenter displacement for the three chosen simulations.

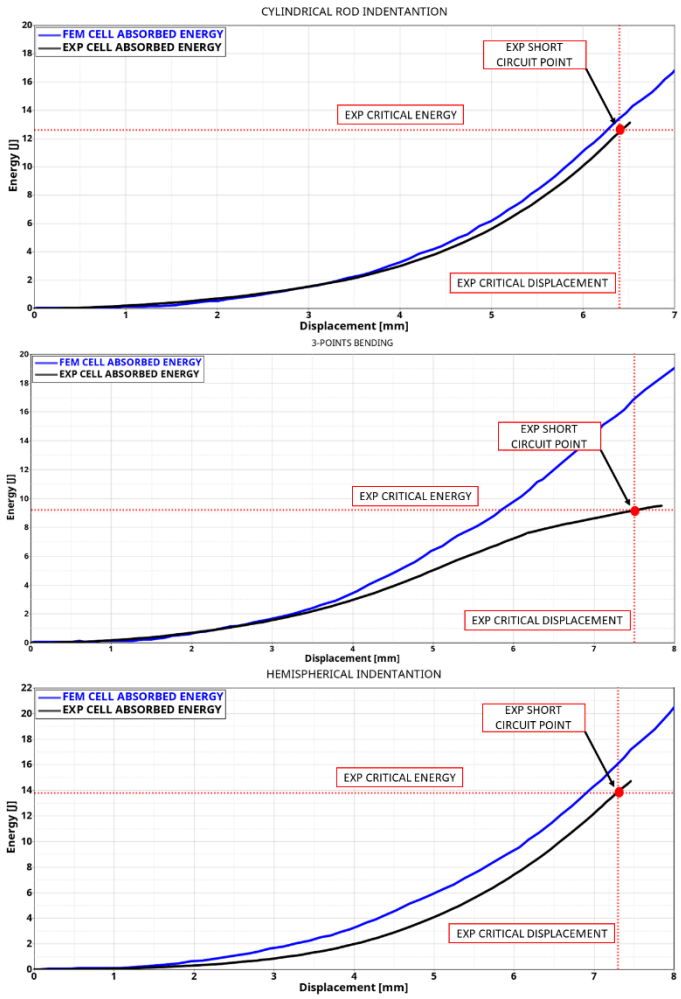

Figure 17. Comparison between experimental [18] and FEM energy vs. displacement for cylindrical rod indentation, 3-points bending and hemispherical indentation respectively.

The experimental values of the energies absorbed by the cells and their critical displacements at the short circuit occurrence are represented by the red dots in the plots. Since the FEM models are not perfectly correlated to the experimental ones, they get to those energies thresholds before reaching the critical displacements. In fact, virtual simulations tend to be stiffer than the experimental results because the indenters displacement are lower at critical short circuit energies. This situation is highlighted in Figure 18, where the virtual deformed shapes are compared with the real test conducted in [18].

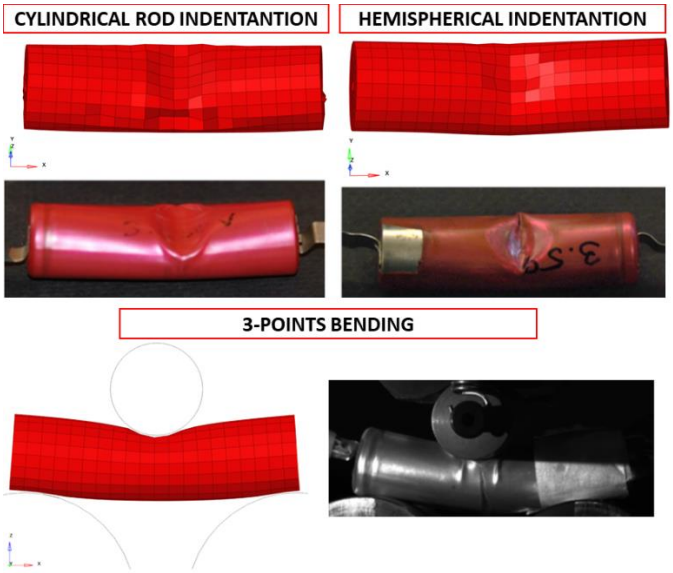

Figure 18. Comparison between experimental [18] and FEM model deformation for cylindrical rod indentation, hemispherical indentation and 3-points bending respectively at the critical energy values.

Therefore, to align the virtual simulations with the real tests, the energy absorption has been chosen as main parameter and the corresponding Von Mises stress has been used as threshold value for the LS-Dyna keyword. The procedure to assess the critical stress value above the three simulations consists in the following steps:

1. Identification of the short circuit point in the experimental energy vs displacement curve (red dots)
2. Projection of the experimental critical energy point to the FEM energy vs displacement curve (blue dots)
3. Application of an additional safety factor of 1.5 to the energy value (yellow dots)
4. Projection of the FEM energy value to the corresponding Von Mises stress (green dots)

In Figure 19, these procedural steps are described graphically.

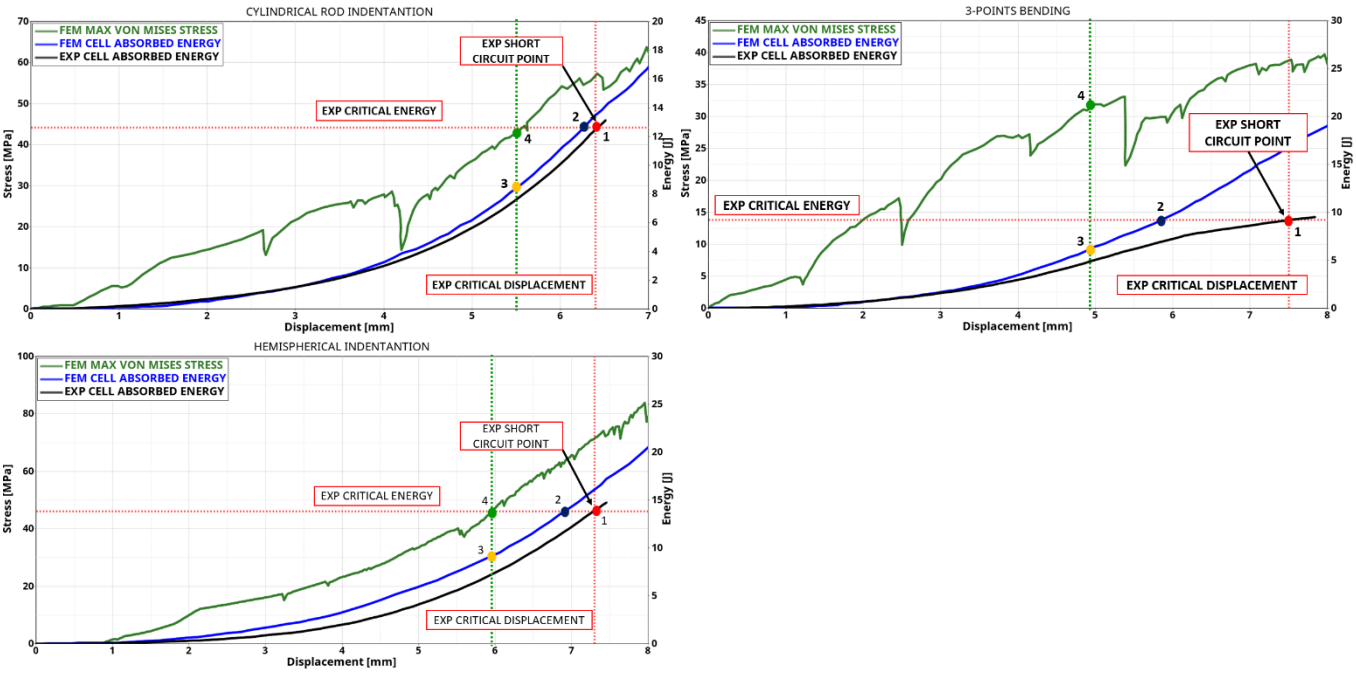

Figure 19. Graphical description of the procedure adopted to define the Von Mises threshold for cylindrical rod indentation, 3-points bending and hemispherical indentation respectively.

In the end, the Von Mises stress represents an equivalent failure index that is easy to evaluate from the simulations' outcomes.
As shown in Table 7, the most stringent condition is the energy absorbed in the three-point bending, because the maximum allowable stress is 31 MPa.

Table 7. Steel and thermal main parameters

	Exp. Energy [J]	**Exp Displacement [mm]**	**Energy with Safety Factor [J]**	**Von Mises [MPa]**
Cylindrical rod Indentation	12,6	6,4	8,4	43
3-points bending	9,2	7,5	6,1	31
Hemispherical indentation	13,9	7,3	9,2	47

Subsequently, the thermo-electro-mechanical model is completed with the thermal properties of the steel and the jellyroll as it is shown in Table 8.

Table 8. Steel and thermal main parameters

	Heat conductivity ($Wm^{-1}K^{-1}$)	**Heat capacity ($Jkg^{-1}K^{-1}$)**
Jellyroll	0.2	1720
Steel	52	502

Figure 20 shows the final thermo-electro-mechanical model of the cylindrical cell during the three-point bending test, using the DEFORMABLE_TO_RIGID_AUTOMATIC keyword to switch the deformable cell to a rigid body when the mechanical impact phenomena end. This keyword is important because it allows high computational cost saving due to the different time constant of the mechanical phenomena and the thermal one.

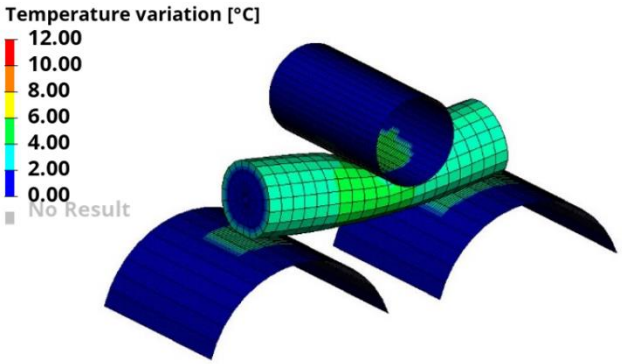

Figure 20. Cell thermo-electro-mechanical model

Complete battery pack simulations

After the calibration of the homogeneous multiphysics cell model, it was implemented into the complete battery pack simulation: the mesh size and the other sensible parameters have been maintained as in the single cell model.
Figure 21 shows the interior part of the battery pack FEM model. All the 500 cells that made up the battery pack and the relative PMMA structures are meshed with 3D solid elements. Instead, the battery pack case, the connecting rods and the screws are modelled with 2D and 1D elements respectively.

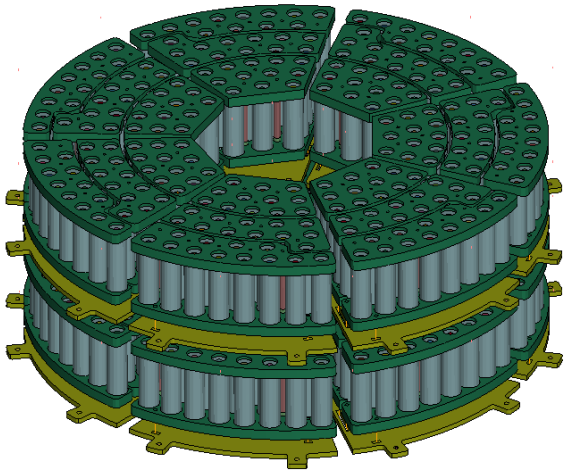

Figure 21. Battery pack active components FEM model

As concerns material data, the mechanical properties of steel and PMMA used into the battery pack are shown in Table 9.

Table 9. Steel and PMMA mechanical parameters

Material	ρ [kg/m3]	E [GPa]	v	A [GPa]	B [GPa]	n
Steel S355jr	7.85e-06	210	0.33	0.355	0.505	0.220
PMMA	1.19e-06	3.06	0.37	0.068	0.031	0.427

The battery pack structural capabilities were validated by simulating of two standard tests, namely the mechanical crushing test of the UNECE R100 and the drop test SAE J2464 [20].
Furthermore, the computational effort was considered by using the same cluster configuration of the cell models to assess the effectiveness of the methodology proposed.

UNECE R100 mechanical crushing simulation

Figure 22 shows the UNECE R100 setup. The test prescribes to gradually push the battery pack against a rigid wall through a stiff crush plate indenter until the force reaches the value of 100 kN.

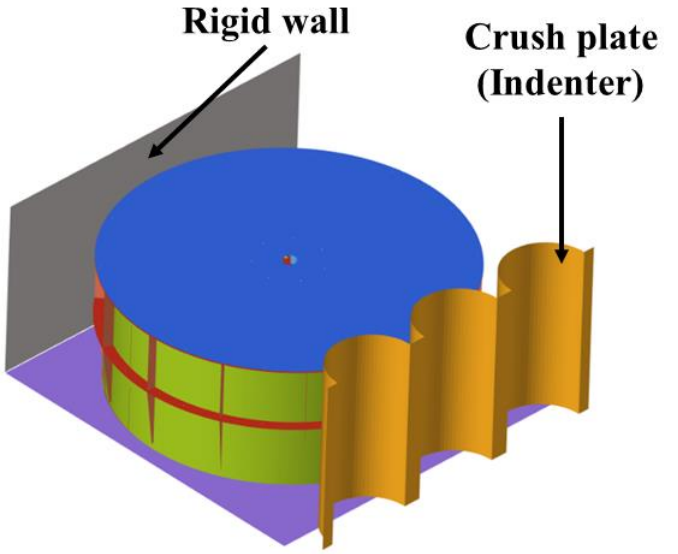

Figure 22. UNECE R100 mechanical crushing FEM model

The crush plate has a dimension of 600x600 mm and a rounded projection with radius of 75 mm. In Figure 23 the trend of the force versus displacement of the UNECE R100 simulation is reported.

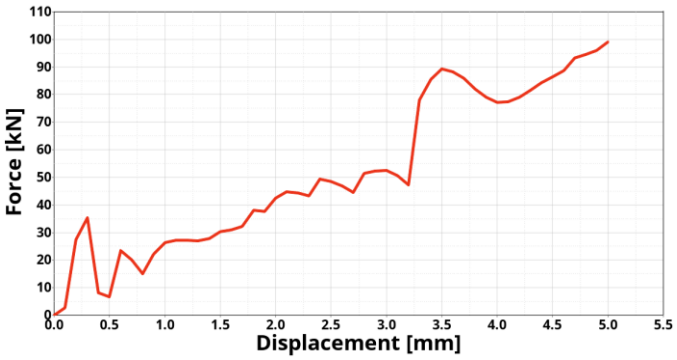

Figure 23. UNECE R100 simulation force vs. displacement

Due to the high complexity of the simulation because two different solvers have been used together (the explicit and the implicit one) and some instabilities related to the thermo-electromagnetic part occurred. Facing these issues, the authors have chosen to present:

- Complete multiphysics cell simulation (already shown in Figure 18) where it is shown the interaction between mechanical stress and its related electro-thermal effects.
- Advanced mechanical simulation of the entire battery pack with homogeneous cell modelling (in the next Figure 25 and 28) where the Von Mises cell stress is compared to threshold to determine a possible short circuit.

The deformed battery pack at the end of the simulation is shown in Figure 24. The external structure absorbed the energy in a very good way, ensuring the right protection to the cells.

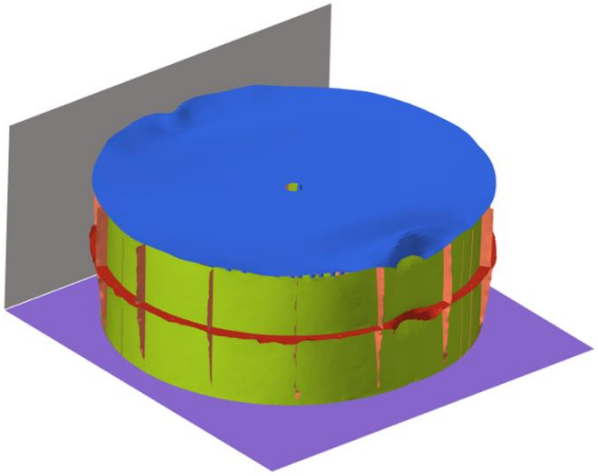

Figure 24. Deformed battery pack during UNECE R100 test simulation

In fact, as shown in Figure 25 jellyroll Von Mises stresses are below 5 MPa almost everywhere and the maximum stress reported is 7 MPa that is abundantly below the threshold of 31 MPa.

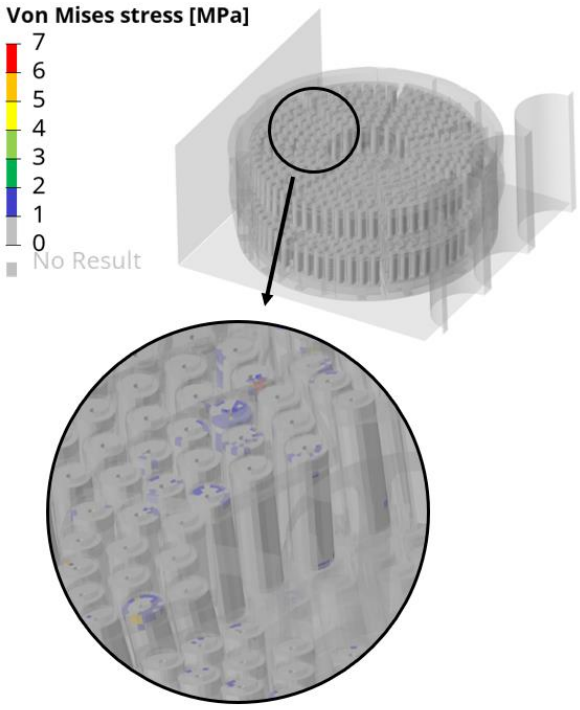

Figure 25. UNECE R100 jellyroll Von Mises stresses distribution

SAE J2464 drop test simulation

For the SAE J2464 test simulation, the same FEM model was used, as shown in Figure 26.

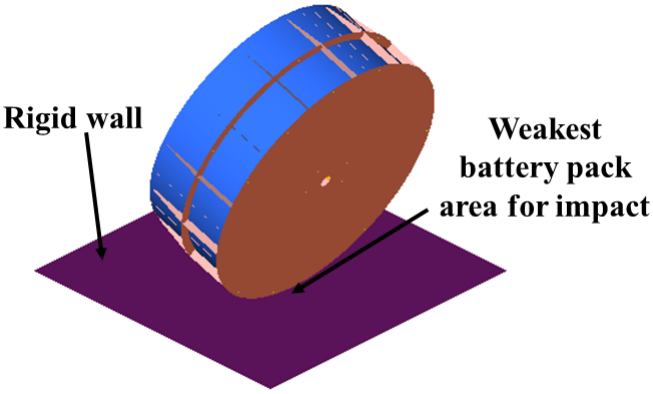

Figure 26. SAE J2464 drop test FEM model

The regulation imposes that the pack must be released from 2 m height and hit a rigid wall in the least favorable position. In the case of the battery pack, the edge between lid and circumferential sheets has been considered the worst place where impact can happen. The initial velocity of 6.26 m/s was set to all the nodes to replicate the effective impact condition, together with the gravity acceleration.
The deformed shape of the battery pack is reported in Figure 27, when the kinetic energy was completely absorbed by the structure.

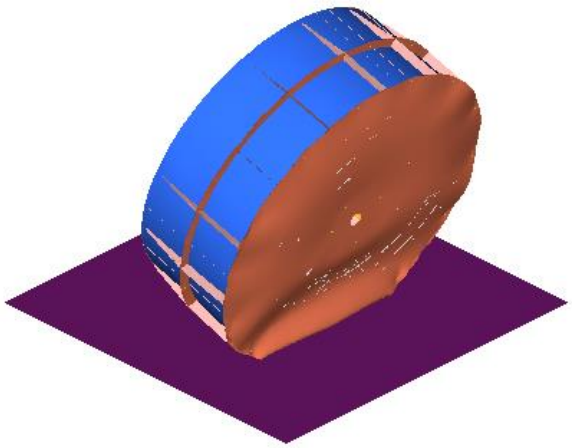

Figure 27. Deformed battery pack during the SAE J2464 test simulation

As in the former simulation, short circuit occurrence has been checked considering the Von Mises stresses at the jellyroll level. As shown in Figure 28, their values are quite lower than the safety threshold because the maximum stress detected is 7 MPa.

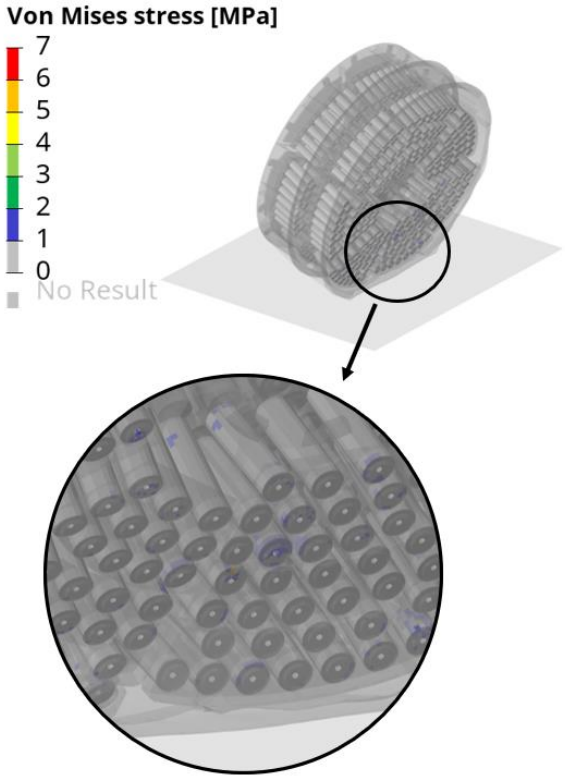

Figure 28. SAE J2464 jellyroll Von Mises stresses distribution

In conclusion, the design of the toroidal battery pack was considered validated and the main safety requirements were satisfied.
The two simulations cases run in reasonable time in the server whose main characteristics are showed in Table 5. In fact, as concerns total simulations time, the SAE J2464 last 4h 16m 13s while the UNECE R100 5h 23m 17s that represent a very good result in terms of computational effort for a full-scale simulation.

Conclusion and future developments

In this paper the design and simulation procedure of a battery pack for a mild-hybrid conversion is presented. A toroidal external shape was defined to fit within the spare wheel space of the most common vehicles.
The electrical reference parameters were defined considering a widespread A-segment city car mission and they were used as reference to define module layout, electric connections and cooling system.
The simulations of the standard homologation test on battery cases represent a complex task due to cell components' small size and the multiphysics dimension of the problem that involve different aspects such as mechanical, thermal and electrical.
For this reason, a novel methodological approach was proposed to cope with the modelling issue and to optimize the computational effort.
Two specific cell modelling methodologies were compared and correlated with three experimental tests found in literature. The homogeneous approach was considered the best trade-off in terms of accuracy level and computational cost.
The generated mechanical cell FE model was coupled with the thermal and the electromagnetic solvers using novel LS-DYNA tools.
In particular, the Von Mises stress was chosen as short circuit threshold, obtained as a combination between experimental and virtual factors in different loading conditions.
However, this choice is not the optimal one, due to the Von Mises variation in consequence of load case configuration. For instance, the use of local strain output may represent a better solution, because they can also be correlated with the

experimental values. Unfortunately, this output request is not yet implemented in the last LS-Dyna version for the thermo-electro-mechanical coupling.
Subsequently, the validated homogenous cell model was reproduced into the full battery pack simulation, and two standard homologation tests were simulated: the UNECE R100 and the SAEJ2464. However, some instabilities arisen in the simulation as result of difficulties to couple the explicit and the implicit solver simultaneously.
For this reason, the short circuit assessment was performed by using the explicit mechanical solver without considering any other effects. Stresses plotted in the jellyroll were compared with the Von Mises threshold and no potential failure was observed. Therefore, the battery pack design has been validated for both tests.
Although this multiphysics approach still presents some instabilities at full-scale level, the methodology proposed could represent an effective innovation in the field of battery pack simulations. In fact, this approach could clear the way for real lightweight case structures thanks to the capabilities to simulate the real behavior of the cells and their failure mechanisms. Moreover, the average calculation time for a complete model is around 4 hours and 30 minutes, that is a reasonable time for a full vehicle scale considering the number of the cells involved and the detail levels. In addition, the Von Mises threshold represents a reliable failure index even if it is not the most accurate one. Finally, there are novel tools are under development by Dynamore and future work could involve several test on complex systems such as battery pack to assess the improvements of the latest solver release. Further works could be focused on improving the material model of the jellyroll, considering the anisotropy and the influence of the SOC on the mechanical properties. In addition, structural optimization could be performed to optimize mass and strength to also increase the specific energy density of the whole pack.

Reference

1. Update of the NDC of the European Union and its Member States, The update of the nationally determined contribution of the European Union and its Member States, Berlin, 17 December 2020
2. News European Parliament, CO2 emissions from cars: facts and figures (infographics), 22 March 2019
3. Climate Action-European Commission, Proposal for Post 2020 CO2 Targets for Cars and Vans, Climate Action-European Commission, Brussels, Belgium, 2017
4. https://www.eyesvehicles.com, Accessed May 2021
5. https://www.retro-ev.com, Accessed May 2021
6. A. Ferraris, F. Micca, A. Messana,A. G. Airale et al, “Feasibility Study of an Innovative Urban Electric-Hybrid Microcar.” *International Journal of Automotive Technology.* Vol 20 (2019): pp.237–46. https://doi.org/10.1007/s12239-019-0023-x.
7. R. Setiawan, M. Rusyad Salim , “Crashworthiness Design for an Electric City Car against Side Pole Impact”, J. Eng. Technol. Sci., Vol. 49, No.5, 2017, 587-603
8. L. Scurtu, I. Szabo, F. Mariasiu, D. Moldovanu, et al., “Numerical analysis of the influence of mechanical stress on the battery pack’s housing of an electric vehicle”, IOP Conference Series: Materials Science and Engineering, 2019
9. J. Kukreja, T. Nguyen, T. Siegmund, W. Chen, et al., “Crash analysis of a conceptual electric vehicle with a damage tolerant battery pack”, Extreme Mechanics Letters 9 (2016) 371-378
10. Regulation No 100 of the Economic Commission for Europe of the United Nations (UN/ECE) – Uniform provisions concerning the approval of vehicles with regard to dpecific requirements for the electric power train, Rev. Dec. 2010
11. Rizzello, A., Scavuzzo, S., Ferraris, A., Airale, A.G. et al, “Electrothermal battery pack model for automotive application: Design and validation”, 12th AEIT International Annual Conference, AEIT 2020, https://doi.org/10.23919/AEITAUTOMOTIVE50086.2020.9307377
12. Rizzello, A., Scavuzzo, S., Ferraris, A., Airale, A.G. et al, “Dynamic Electro-Thermal Li-ion Battery Model for Control Algorithms”, 12th AEIT International Annual Conference, AEIT 2020, https://doi.org/10.23919/AEIT50178.2020.9241107
13. Mohammed Yusuf Ali, Wei-Jen Lai, Jwo Pan, “Computational models for simulations of lithium-ion battery cells under constrained compression tests”, Journal of Power Sources 273 (2015) 448-459, September 2014

14. Chao Zhang, Shriram Santhanagopalan, Michael A. Sprague, Ahmad A. Pesaran, “Coupled mechanical-electrical-thermal modelling for short-circuit prediction in a lithium-ion cell under mechanical abuse” Journal of Power Source 242 (2013) 325-340, May 2013
15. Young Xia, Qing Zhou, “Mechanical Behaviour of Lithium-Ion Battery Component Materials and Error Source Analysis for test Results”, SAE Technical Paper 2016-01-0400, 2016, doi:10.4271/2016-01-0400.
16. Lars Greve, Clements Fehrenbach, “Mechanical testing and macro-mechanical finite element simulation of the deformation, fracture, and short circuit initiation of cylindrical Lithium-ion battery cells”, Journal of Power Sources 214 (2012) 377-385, April 2012
17. Ilya Avdeev, Mehdi Gilaki, “Structural analysis and experimental characterization of cylindrical lithium-ion battery cells subjected to lateral impact”, Journal of Power Sources 271 (2014) 382-39, August 2014
18. Elham Saharaei, John Campbell, Tomasz Wierzbicki, “Modelling and short circuit detection of 18650 Li-ion cells under mechanical abuse conditions”, Journal of Power Sources 220 (2012) 360-372, August 2012
19. Jun Xu, Binghe Liu, Xinyi Wang, Dayong Hu, “Computational model of 18650 lithium-ion battery with coupled strain rate and SOC dependencies”, Applied Energy, June 2016
20. Electric and Hybrid Electric Vehicle Rechargeable Energy Storage System (RESS) Safety and Abuse Testing, SAE Standard J2464_200911, Rev. Nov. 2011.

Contact Information

Corresponding Authors:
Alessandro Messana, Politecnico di Torino, Department of Mechanical and Aerospace Engineering (DIMEAS), alessandro.messana@polito.it

Acknowledgment

The authors want to thank for the helpful and continuous support Dynamore for FEM software advice and suggestions, BETA CAE Italy for the pre-processor software and Corinne Getti for the experience and the technical support on LS-Dyna. The research has been conducted with the own funds of the research group IEHV (Innovative Electric and Hybrid Vehicles) and in cooperation with Beond s.r.l.